Supporting Information

Regulation of Nitrogen Configurations and Content in 3D Porous Carbons for Improved Lithium Storage

Huixia Chao*, Yifan Zhu，Xiangsheng Luo, Chaoqun Zhang, Jiale Liu, Weijiang Wang, Meiqing Qu

Guangxi Colleges and Universities Key Laboratory of Beibu Gulf Oil and Natural Gas Resource Effective Utilization, Qinzhou Key Laboratory for Development and Application of High Performance Functional Materials, Beibu Gulf University, Qinzhou, 535011, China

Keywords: N-doping, Pyrrolic-N, Pyridinic-N, Pseudocapacitive contribution, Lithium storage

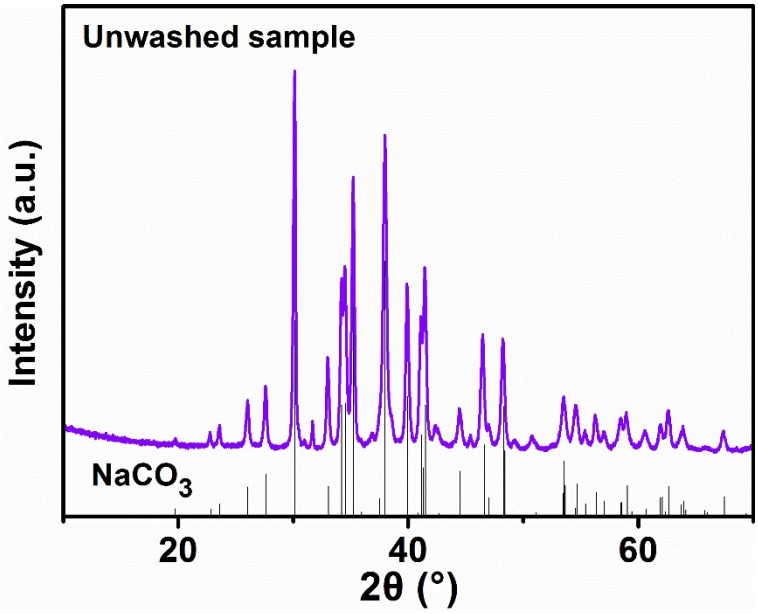

Figure S1. XRD pattern of CN-6 before washing.

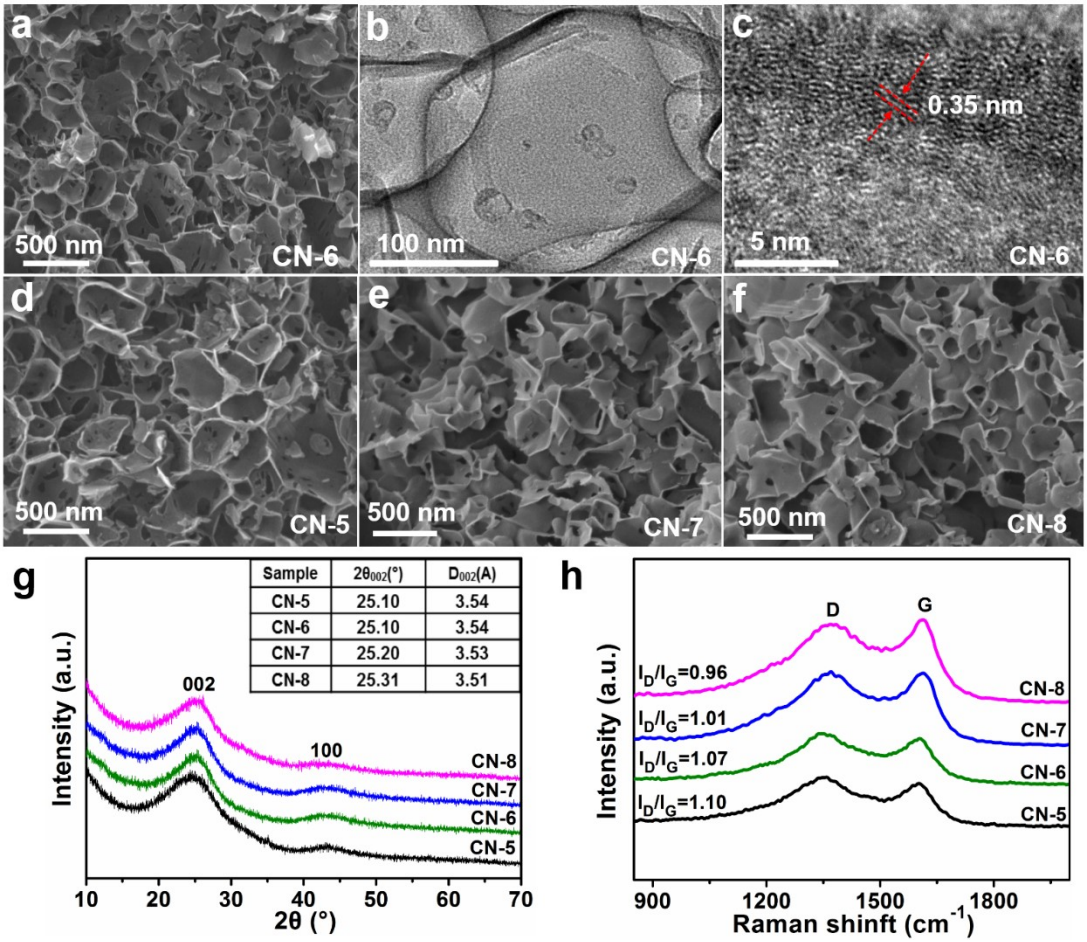

Figure S2. (a) SEM image of CN-6. (b-c) TEM images of CN-6 at different magnification. SEM images of (d) CN-5, (e) CN-7, and (f) CN-8. (g) XRD patterns and (h) Raman spectra of the CNs obtained at different temperatures.

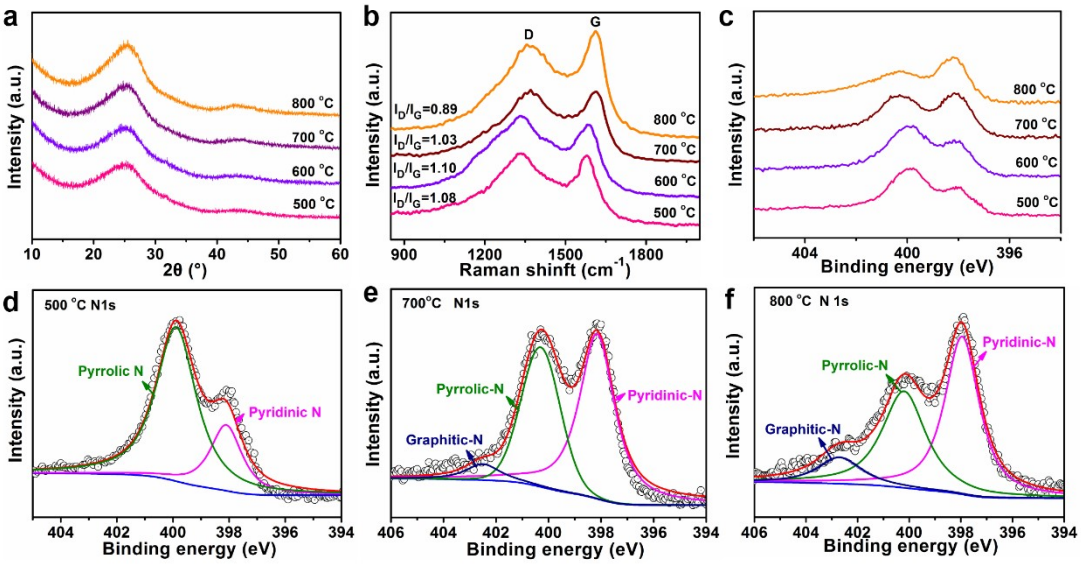

Figure S3. (a) XRD patterns, (b) Raman spectra, and (c) XPS of N-doped CN-6 with the same N doping level of around 4.0 at.% obtained at different temperatures. High-resolution XPS N 1s spectra of N-doped CN-6 obtained at different temperatures: (d) 500 °C, (e) 700 °C, and (f) 800 °C.

Temperature, °C	N-content, at.%	Pyrrolic-N, at.%	Pyridinic-N, at.%	Graphitic-N, at.%
500	4.1	74.7	25.3	0
600	4.1	69.5	26.1	4.4
700	4.1	47.3	45.5	7.2
800	4.0	38.6	50.8	10.6

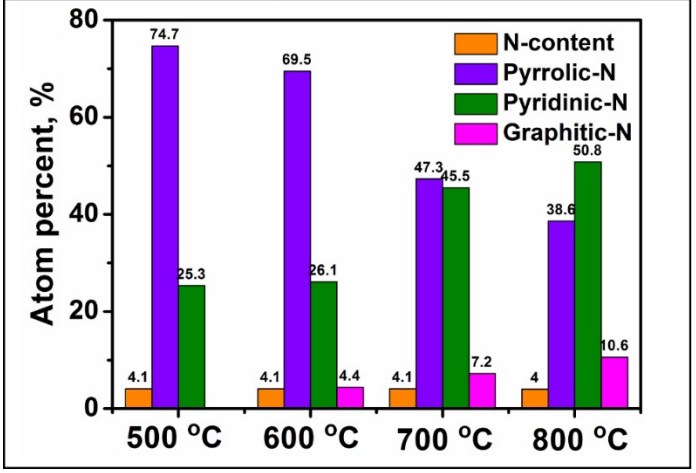

Figure S4. Nitrogen configurations correlated with heat temperatures.

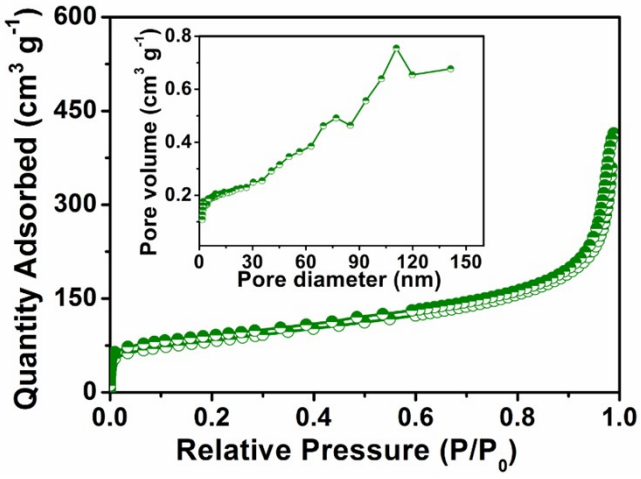

Figure S5. BET results of NCN-10.

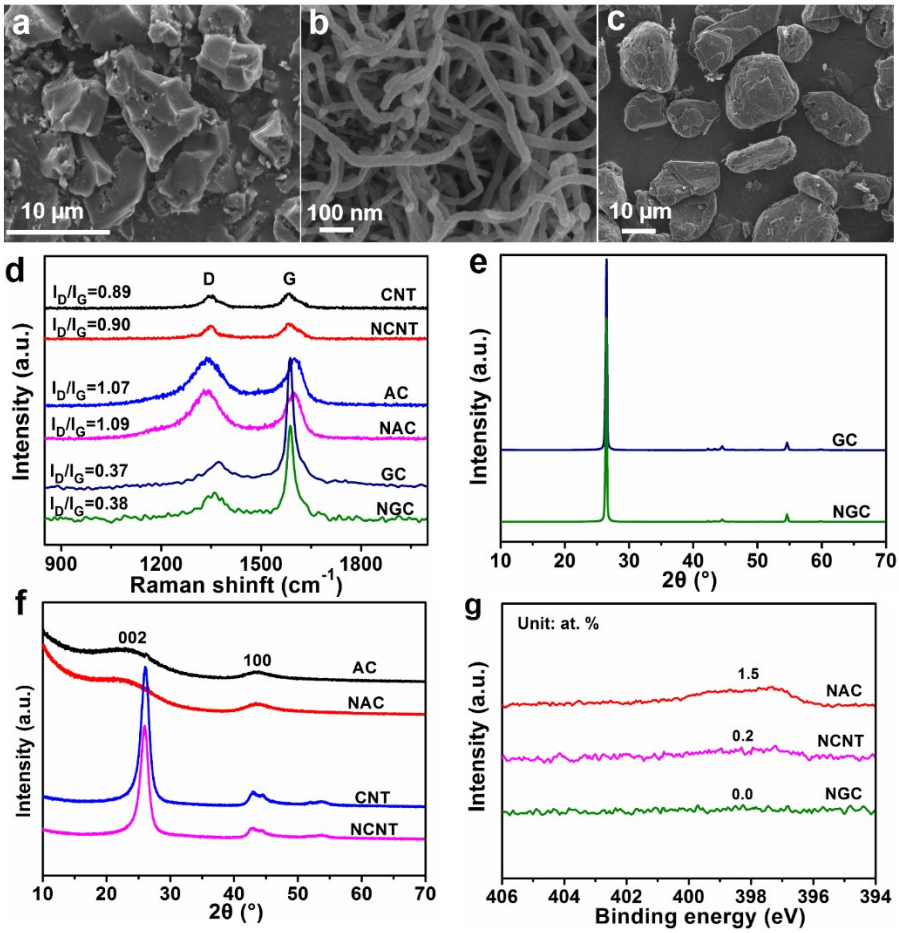

Figure S6. SEM images of (a) AC, (b) CNTs, and (c) graphitic carbon (GC). (d) Raman spectra of AC, CNTs, GC before and after N-doping. (e) XRD pattern of GC before and after N-doping. (f) XRD patterns of AC and CNTs before and after N-doping. (g) XPS of AC, CNTs and GC after N-doping.

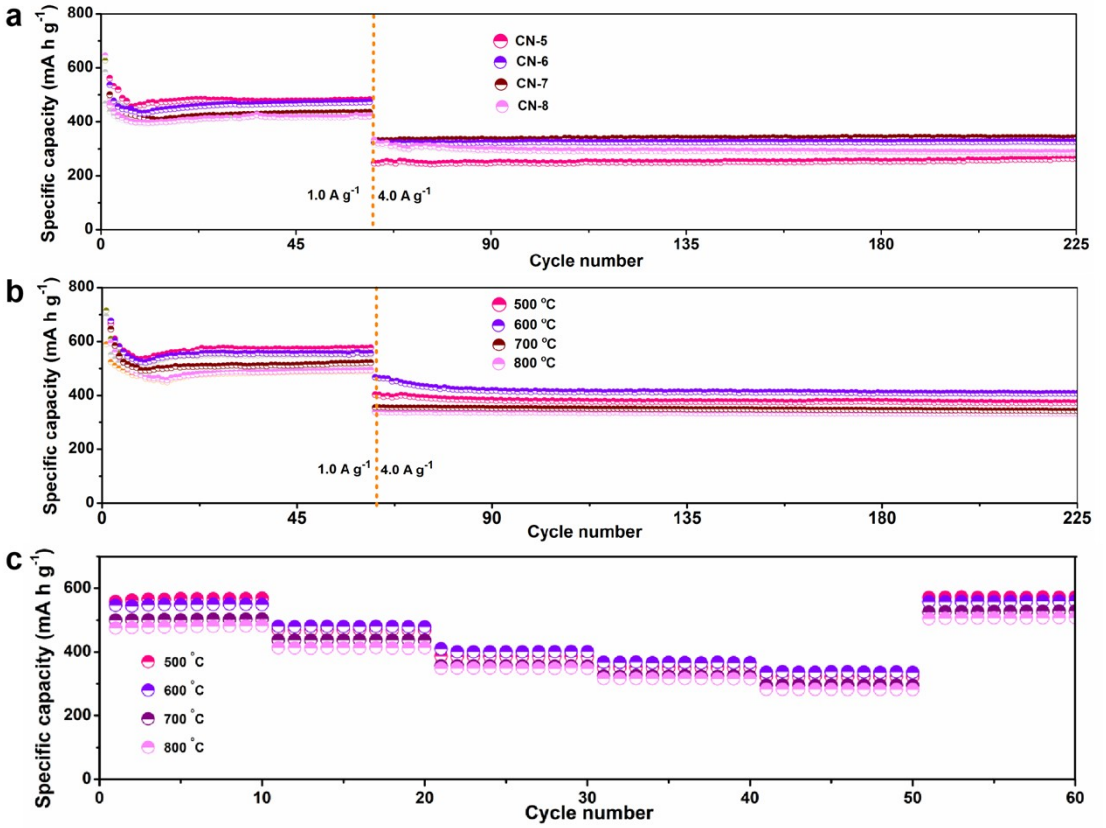

Figure S7. Cycling performance of (a) CNs and (b) N-doped CN-6 at different temperature at 1.0 A g^{-1} and 4.0 A g^{-1} for lithium storage. (c) Rate capability of N-doped CN-6 at different temperature.

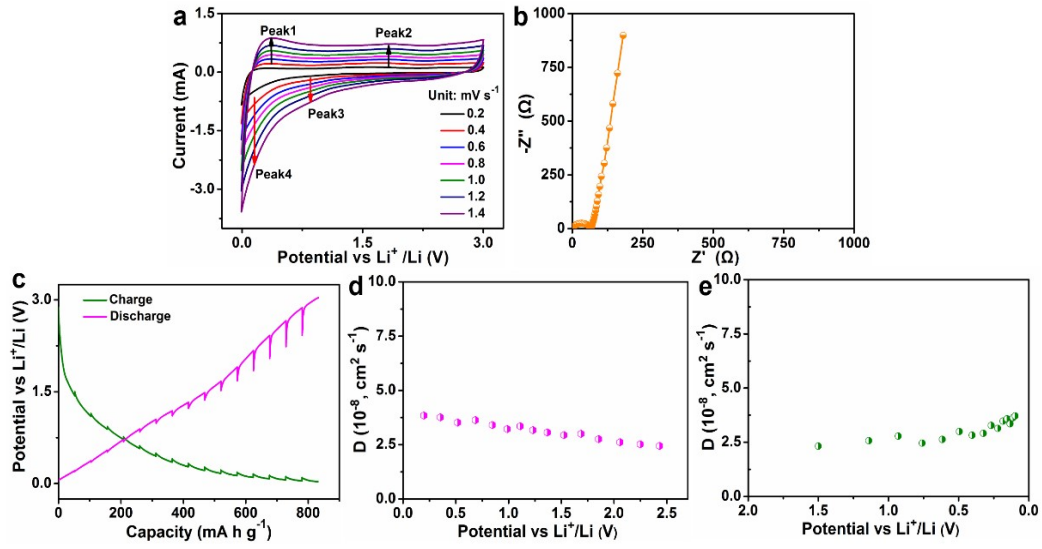

Figure S8. Electrochemical performance of NCN-10 for lithium storage. (a) CV tests at varying scan rates from 0.2 to 1.4 mV s^{-1}. (b) Nyquist plot recorded with a fresh half-cell at 2.6 V vs. Li/Li^+. (c) GITT measurement and the diffusivity coefficient during (d) discharge and (e) charge for the half-cell.

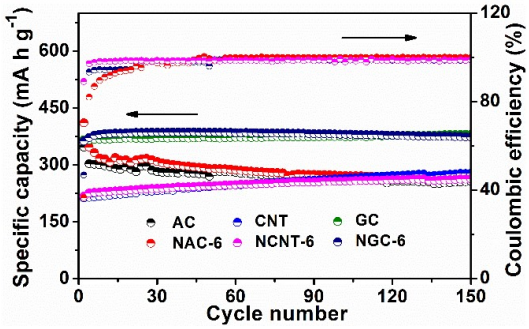

Figure S9. Cycling performance of AC, CNTs, and graphite before and after N-doping at 1.0 A g^{-1} for lithium storage.

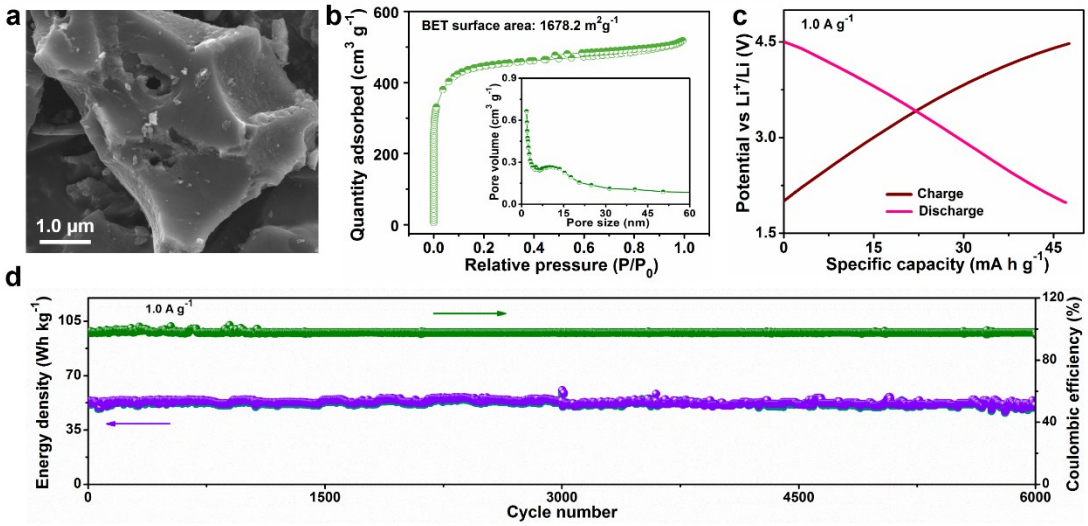

Figure S10. Structure and electrochemical characterization of the AC cathode. (a) SEM image, (b) Nitrogen-sorption isotherm of the AC, inset in (b) is the pore-size distribution. (c) GCD profiles within the potential range 2.0–4.5 V *vs* Li^+/Li at 1.0 A g^{-1}. (d) Cycling performance evaluated at 1.0 A g^{-1} for lithium storage.

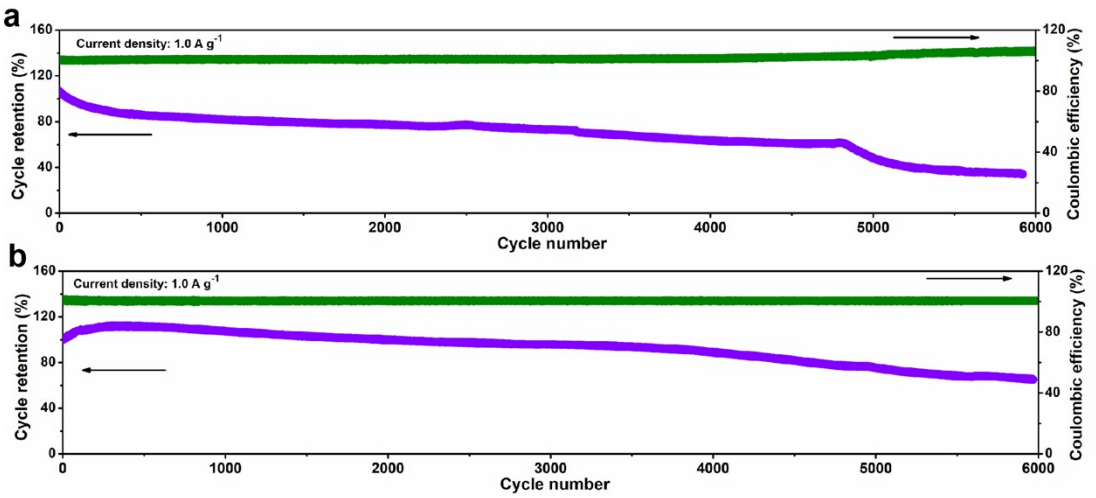

Figure S11. Cycling performances of the LICs for AC/NCN-10 mass ratios of (c) 2.0 and (d) 4.0.